Available online at www.sciencedirect.com
ScienceDirect
Trans. Nonferrous Met. Soc. China 30(2020) 2658−2668
Transactions of Nonferrous Metals Society of China
www.tnmsc.cn

Effects of deformation parameters on microstructure and texture of Mg−Zn−Ce alloy

Yu-zhou DU[1,2], Dong-jie LIU[1,2], Yan-feng GE[1,2], Bai-ling JIANG[1,2]

1. School of Materials Science and Engineering, Xi'an University of Technology, Xi'an 710048, China;
2. Shaanxi Provincial Engineering Research Center for Magnesium Alloys,
Xi'an University of Technology, Xi'an 710048, China

Received 10 February 2020; accepted 30 July 2020

Abstract: Compression tests were performed on the Mg−6Zn−0.5Ce (wt.%) alloy using a Gleeble−1500 thermo-mechanical simulator testing system at temperatures of 250, 300, 350 °C and strain rates of 0.001, 0.01, 0.1 s^{-1}. The microstructure and texture evolution of the Mg−6Zn−0.5Ce alloy during hot compression were investigated by optical microscopy (OM) and electron backscattered diffraction (EBSD). The results showed that Zener−Hollomon parameters obtained from the deformation processes had a significant effect on the dynamic recrystallization and texture of the Mg−6Zn−0.5Ce alloy. The fraction of undynamically recrystallized (unDRXed) regions increased, and the dynamically recrystallized (DRXed) grain size decreased with increasing the Zener−Hollomon parameters. The texture intensity of the DRXed regions was weaker compared with that in the unDRXed regions, which resulted in a sharper texture intensity in the samples deformed with higher Zener−Hollomon parameters. The increase in recrystallized texture intensity was related to preferred grain growth.

Key words: Mg−Zn−Ce alloy; hot deformation; texture evolution; dynamic recrystallization

1 Introduction

Mg and its alloys offer a remarkable potential for applications in the automotive, defense and electronic industries due to their low density, good castability and superior machinability [1]. The poor mechanical response of the as-cast Mg alloys restricts their wide usage [2]. Thermo-mechanical processes are capable of modifying microstructure through dynamic recrystallization (DRX), which can improve the strength of Mg alloys [3]. However, wrought Mg alloys always exhibit a sharp basal texture [4], which is a result of their hexagonal close-packed (HCP) structure. Consequently, mechanical anisotropy and poor formability are commonly accompanied after the deformation of Mg alloys [4]. Therefore, textural modification of wrought Mg alloys has become a hot topic in recent decades [5].

It has been reported that microalloying is a successful approach to randomize Mg alloy texture [6,7]. BALL and PRANGNELL [8] first found that WE54 alloy extrusion exhibited a weaker texture compared with rare earth (RE)-free alloys. Subsequently, RE elements have been observed to affect the conventional texture in Mg alloys after recrystallization [9]. A threshold concentration of RE element addition is required for the formation of RE texture components in Mg alloys [10]. HANTZSCHE et al [11] proposed that the amount limitations of RE required to modify texture were associated with the solid solubility of the respective elements in the Mg alloys [11]. However, recent

---

Foundation item: Project (51801150) supported by the National Natural Science Foundation of China; Project (2019JQ-512) supported by the Shaanxi Natural Science Basic Research Program, China; Project (16JK1557) supported by the Shaanxi Provincial Department of Education Fund, China

Corresponding author: Yu-zhou DU; Tel: +86-29-82312516; E-mail: duyuzhou@xaut.edu.cn

DOI: 10.1016/S1003-6326(20)65410-3

studies have reported that the resulting texture after dynamic recrystallization in RE containing Mg alloys has also been influenced by deformation parameters [12,13]. For example, ROBSON et al [13] found an unusual texture component in the Mg−6Y−7Gd−0.5Zr (wt.%) alloy when extruding with a high extrusion ratio [13]. The inhibition of shear bands deformed at high temperature resulted in the disappearance of the RE texture component in the Mg−Gd binary alloy [14], but the RE texture component in the Mg−Zn−Ce alloy was prohibited when extruding at low temperature (300 °C) due to the inhibition of the activation of the $\langle c+a \rangle$ slip system [15]. High strain rate also played an essential role in RE formation in Mg−0.23wt.%Ce alloy, because the high deformation speed provided great deformation-induced stored energy for the dynamic recrystallization process [16]. Therefore, the texture development during dynamic recrystallization is associated with chemical compositions and deformation parameters. However, there is still a lack of the effect of deformation parameters on the texture of RE containing Mg alloys.

Unraveling the relationship between the processing conditions and the microstructure can provide guidelines to produce a desirable microstructure for Mg alloys. Mg−Zn based alloys are promising candidates for commercial applications. Ce is an important alloying element in Mg alloys [17]. Generally, a small addition of Ce is enough to reduce the texture intensity of wrought Mg alloys [18]. Therefore, 0.5 wt.% Ce was added in the present study, and Mg−6Zn−0.5Ce (wt.%) alloys were deformed under various deformation parameters to identify the influence of deformation parameters on microstructural evolution and texture. The aim of the present study is to provide a way to fabricate high performance RE-containing Mg alloys with high strength and ductility.

2 Experimental

The Mg−6Zn−0.5Ce (wt.%) alloys were fabricated by melting pure Mg, pure Zn and Mg−30%Ce master alloys at 750 °C with the protection of a mixed atmosphere of CO_2 and SF_6. The casting ingots were homogenized at 350 °C for 12 h. After that, cylindrical samples with diameters of 8 mm and heights of 12 mm were machined from the homogenized alloys and used in compression tests. The compression tests were carried out on a Gleeble−1500 thermo-mechanical simulator testing system. The specimens were uniaxially compressed to a height reduction of 60% (corresponding to a true strain of 0.9) at strain rates of 0.001−0.1 s^{-1} and temperatures of 250−350 °C. The compressed specimens were immediately quenched into water to preserve the deformed microstructure. For each condition of deformation, at least three samples were repeated to ensure reproducibility.

Specimens for microstructural observation and texture were cut from the central part of the section parallel to the compression direction. The volume fraction of the deformed region was measured according to the area ratio of the extruded alloys using Image Pro 5.0 software. Electron backscattered diffraction (EBSD) tests were conducted on a scanning electron microscope (SEM) with an HKL-EBSD system under accelerating voltage of 20 kV. The acquired EBSD data with band contrast larger than 20 were used to calculate pole figures using the software of the MTEX toolbox [19]. The step sizes for the EBSD tests were 0.7−2 μm according to the DRXed grain size of the compressed samples.

3 Results and discussion

3.1 Compressive stress−strain curves and deformation activation energy

Figure 1 presents the SEM images of the as-cast and homogenized alloys. A large amount of semi-continuous second phases distributing along grain boundaries were observed in the as-cast alloy (Fig. 1(a)). The semi-continuous second phases became discrete for the homogenized alloy (Fig. 1(b)), indicating that the second phases were partially dissolved into the matrix. The EDS results of the second phase are shown in Fig. 1(c). It could be seen that the second phase contained about 43.73 at.% Zn, 7.92 at.% Ce, and 48.35 at.% Mg. A *T* phase with a composition of 7.7 at.% Ce, 19.3−43.6 at.% Zn in the Mg−Zn−Ce alloy was obtained at 350 °C [20]. The second phase in the rapidly solidified Mg−8Zn−MM alloy was determined to be $Mg_{52.6}Zn_{39.5}MM_{7.9}$, which was also called a *T* phase [21]. The difference in chemical composition of the second phase between the previous investigation and the present study was

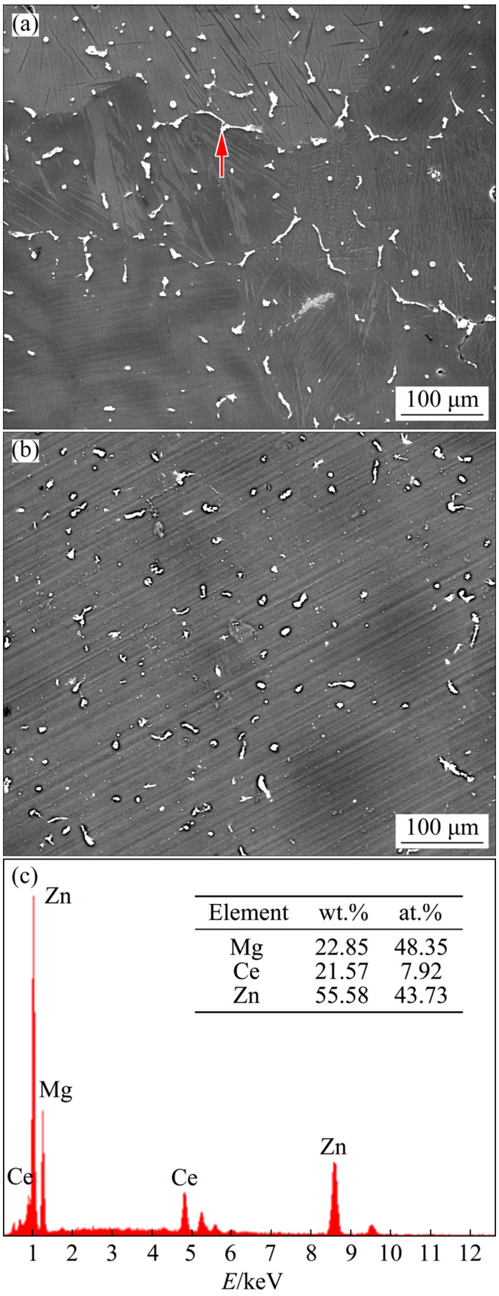

Element	wt.%	at.%
Mg	22.85	48.35
Ce	21.57	7.92
Zn	55.58	43.73

Fig. 1 SEM images of as-cast (a), homogenized (b) Mg−6Zn−0.5Ce (wt.%) alloys and EDS results (c) of second phases arrowed in (a)

because the EDS results were affected by the surrounding Mg matrix due to its relatively large area and depth for analysis. Hence, the second phase in the Mg−6Zn−0.5Ce (wt.%) alloy was inferred to be a *T* phase in the present study.

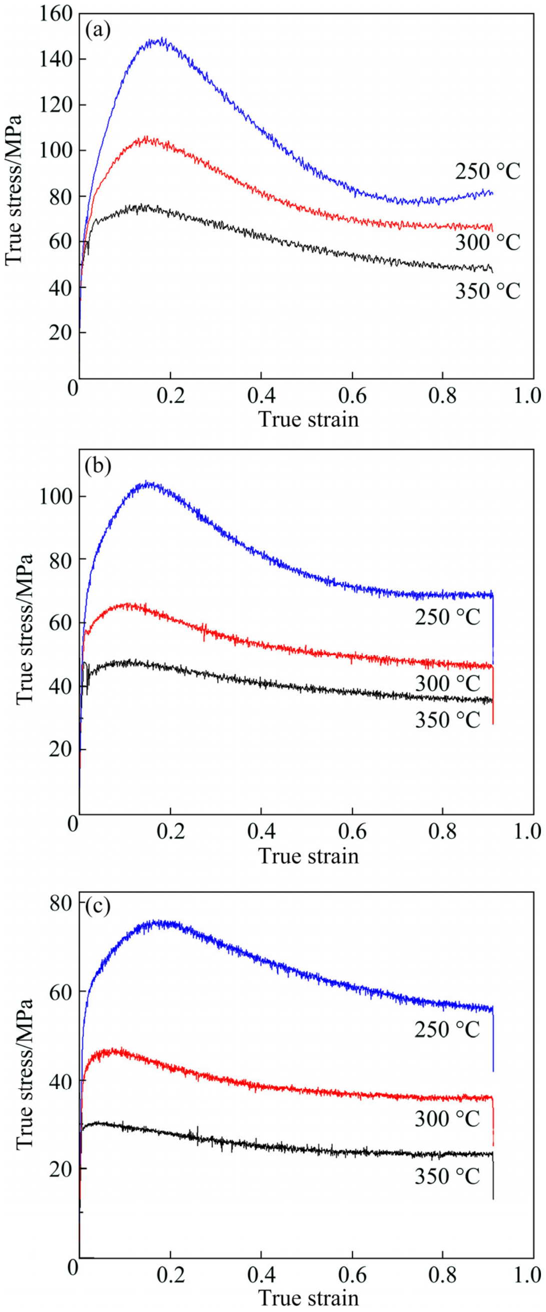

Fig. 2 True stress−true strain curves of samples compressed at different strain rates: (a) 0.1 s^{-1}; (b) 0.01 s^{-1}; (c) 0.001 s^{-1}

Figure 2 shows the true stress−true strain curves of the homogenized alloys after compression. All curves showed similar flow deformation behavior, i.e., the flow stress first increased to a maximum and then decreased to a steady state, which was typical characteristic of the dynamic recrystallization [22]. At the beginning of the deformation, the hardening rate was higher than the softening rate, which resulted in a sharp rise of flow stress with increasing strain. With further deformation, the softening effect from dynamic recrystallization exceeded the hardening effect during deformation, which gave rise to a decrease in flow stress. When a dynamic balance between softening and hardening reached, flow stress showed a steady state. Additionally, it could be observed that the peak of flow stress and corresponding strain were reduced with increasing deformation temperature and decreasing strain rate. Higher temperature provided higher dislocation mobility and lower strain rate, which could provide longer time for activation energy accumulation and was beneficial to the softening process.

Deformation activation energy is typically used to characterize the difficulty of the hot deformation process, which can be determined by the Arrhenius equations [23]:

$$\dot{\varepsilon} = A_1\sigma^{n_1}\exp[-Q/(RT)] \tag{1}$$

$$\dot{\varepsilon} = A_2\exp(\beta\sigma)\exp[-Q/(RT)] \tag{2}$$

$$\dot{\varepsilon} = A[\sinh(\alpha\sigma)]^n\exp[-Q/(RT)] \tag{3}$$

where Q is deformation activation energy (kJ/mol), $\dot{\varepsilon}$ is the strain rate (s^{-1}), σ is the flow stress (MPa), R is the mole gas constant (8.314 J/(mol·K)), T is the thermodynamic temperature (K), and A_1, A_2, A, n_1, n, β and α are material constants ($\alpha=\beta/n_1$).

From Eqs. (1)−(3), the material constants n_1 and β can be calculated as

$$n_1 = \left(\frac{\partial\ln\dot{\varepsilon}}{\partial\ln\sigma}\right)_T \tag{4}$$

$$\beta = \left(\frac{\partial\ln\dot{\varepsilon}}{\partial\sigma}\right)_T \tag{5}$$

Then, the values of n_1 and β were determined by measuring the slopes of the $\ln\dot{\varepsilon}-\ln\sigma$ and $\ln\dot{\varepsilon}-\sigma$ curves at each temperature, respectively. Figure 3 shows the linear relationship of $\ln\dot{\varepsilon}-\ln\sigma$ and $\ln\dot{\varepsilon}-\sigma$ at different temperatures obtained by linear fitting. The average values of n_1 and β were calculated to be 5.797 and 0.079. Then, the value of α of the alloy was determined as $\alpha=\beta/n_1=0.0136$.

The activation energy can be calculated by the hyperbolic sine law according to Eq. (6)

$$Q = R\left\{\frac{\partial\ln\dot{\varepsilon}}{\partial\ln[\sin(\alpha\sigma)]}\right\}_T\left\{\frac{\partial\ln[\sin(\alpha\sigma)]}{\partial(1/T)}\right\}_{\dot{\varepsilon}} \tag{6}$$

Figure 4 shows the linear relationships of $\ln\dot{\varepsilon}-\ln[\sinh(\alpha\sigma)]$ and $\ln[\sinh(\alpha\sigma)]-1/T$. Then, the average activation energy (Q) for the Mg−6Zn−0.5Ce (wt.%) alloy was determined to be

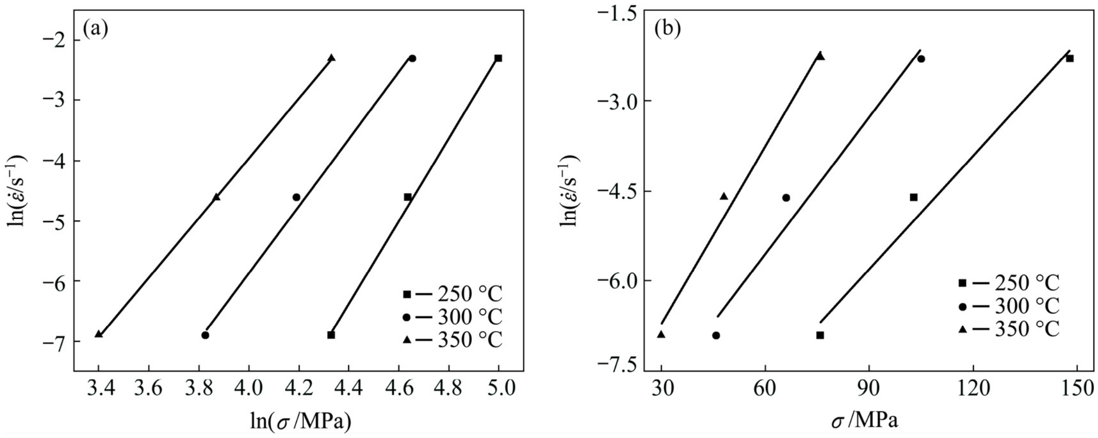

Fig. 3 Variation of $\ln\dot{\varepsilon}-\ln\sigma$ (a) and $\ln\dot{\varepsilon}-\sigma$ (b) at different temperatures

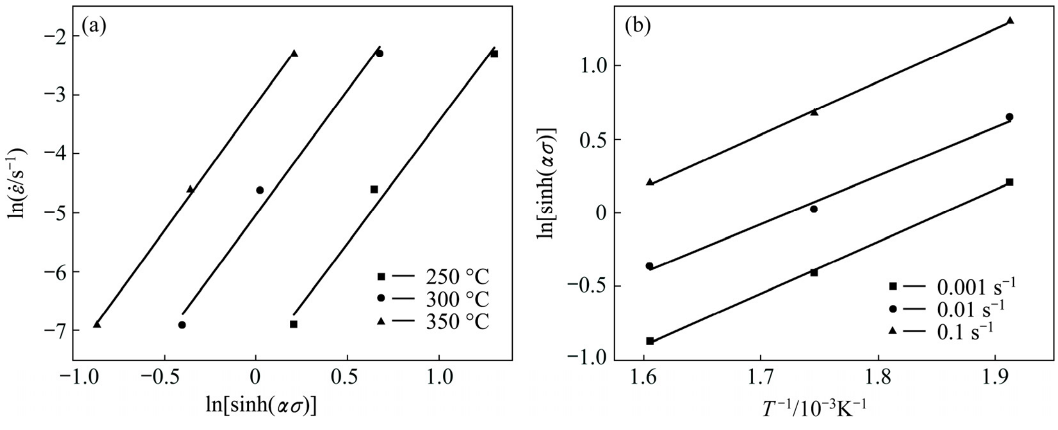

Fig. 4 Variation of $\ln\dot{\varepsilon}-\ln[\sinh(\alpha\sigma)]$ at different temperatures (a) and $\ln[\sinh(\alpha\sigma)]-1/T$ at different strain rates (b)

120.88 kJ/mol, which is close to the lattice self-diffusion activation energy of Mg (Q_{sd}= 135 kJ/mol) [24]. The Q values were reported to be 123−164 kJ/mol for the AZ31 alloy [25−28], 152 kJ/mol for the AZ61 alloy [29], 154 kJ/mol for the AZ80 alloy [30], 176 kJ/mol for the AZ91 alloy [31], and 160−175 kJ/mol for ZK60 alloy [32]. The Q values of Mg alloys are related to the microstructure. Fine precipitates could effectively inhibit dislocation movement during deformation, and fine grains providing more grain boundaries could act as barriers to lattice self-diffusion. Additionally, the addition of alloying elements hinders the movement of dislocation, which leads to the increase in flow stress and activation energy. For the Mg−6Zn−0.5Ce (wt.%) alloy in the present study, Ce mainly existed in the form of the Mg−Zn−Ce (T) phase, and only Zn existed in the form of solute in the Mg matrix. The diffusion velocity would be expected to be similar for Mg and Zn atoms due to similar atomic radius. Therefore, the Q value of the Mg−Zn−Ce alloy was almost the same as the lattice self-diffusion activation energy of Mg. This indicated that the DRX of the Mg−6Zn−0.5Ce (wt.%) alloy was controlled by lattice self-diffusion.

The deformation activation energy could be used to derive the Zener−Hollomon (Z) parameter, which combined the effects of deformation temperature and strain rate on the deformation behavior and is given by the following equation:

$$Z=\dot{\varepsilon}\exp[Q/(RT)] \tag{7}$$

The Zener−Hollomon parameters for the samples in the present study are shown in Table 1.

Table 1 Zener−Hollomon parameters corresponding to different deformation parameters

Sample No.	T/°C	$\dot{\varepsilon}$ /s^{-1}	ln Z
1	250	0.001	20.89
2	250	0.01	23.19
3	250	0.1	25.5
4	300	0.001	18.47
5	300	0.01	20.77
6	300	0.1	23.07
7	350	0.001	16.43
8	350	0.01	18.73
9	350	0.1	21.04

3.2 Microstructural evolution with Zener−Hollomon parameters

Figure 5 shows the optical images of the

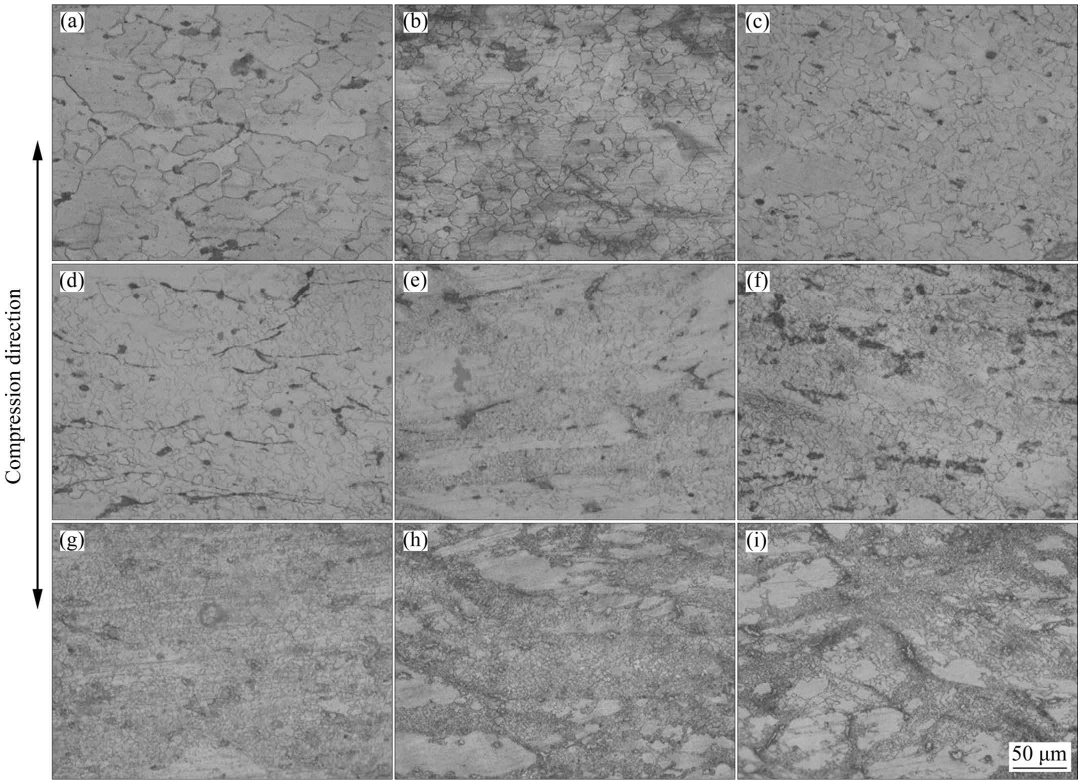

Fig. 5 Optical images of compressed samples with different Zener−Hollomon parameters: (a) ln Z=16.43; (b) ln Z= 18.47; (c) ln Z=18.73; (d) ln Z=20.77; (e) ln Z=20.89; (f) ln Z=21.04; (g) ln Z=23.07; (h) ln Z=23.19; (i) ln Z=25.5

compressed alloys. It is clearly observed that the samples deformed with high Z parameters show a heterogeneous microstructure containing fine DRXed grains and coarse unDRXed regions. The unDRXed region decreased and the DRXed region increased gradually with decreasing Z value. The samples with low Z values ($\ln Z<20$) showed an almost fully recrystallized microstructure (Figs. 5(a−c)).

To further analyze the influence of Z parameters on dynamic recrystallization, the fraction of DRXed region was statistically analyzed using Image Pro software, as shown in Fig. 6. The fraction of DRXed region increased with decreasing $\ln Z$ value, which indicated that high temperature and low strain rate promoted the dynamic recrystallization process. High deformation temperature provided more thermal energy and low strain rate supplied more deformation time for dislocation movement, which gave rise to a high degree of dynamic recrystallization.

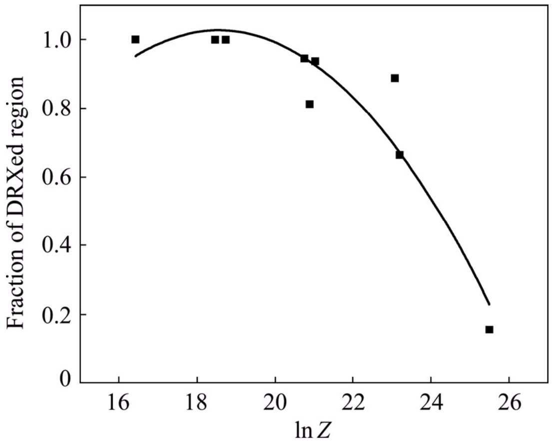

Fig. 6 Variation of fraction of DRXed region with different Zener−Hollomon parameters

Figure 7 shows the variation of DRXed grain size as a function of Z parameter for the specimens compressed to a strain of 60%. WATANABE et al [33] suggested that the DRXed grain size is closely related to the Z parameter, which could be expressed as follows:

$$Zd_{\mathrm{rec}}^{m}=A \tag{8}$$

where d_{rec} is the average DRXed grain size, m is the grain size exponent and A is a constant. It is easy to derive the following relationship:

$$\ln d_{\mathrm{rec}}=\ln A/m-\ln Z/m \tag{9}$$

It could be seen from Fig. 7 that $\ln d_{\mathrm{rec}}$ and $\ln Z$ show a linear relationship, indicating that the factors affecting the DRXed grain size are similar in the present processing regimes [34].

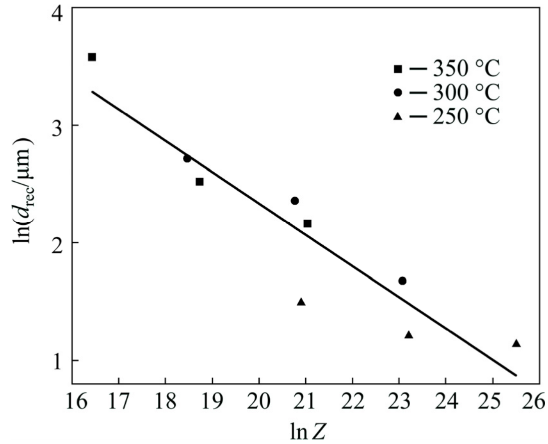

Fig. 7 Variation of DRXed grain size with Z parameter at different temperatures

3.3 Relationship between texture and Zener−Hollomon parameter

The degree of dynamic recrystallization and DRXed grain size both increased with decreasing Z values, as mentioned in Section 3.2. To investigate the texture of the Mg−Zn−Ce alloy under different deformation conditions, samples with different Z parameters were analyzed using EBSD. Figure 8 shows the EBSD results of the specimens deformed with different Z parameters. Crystallographic orientations are represented by different colors, as defined in the inverse pole figure (IPF). The samples deformed with high Z parameters exhibited a heterogeneous microstructure with fine DRXed grains and coarse unDRXed region (Figs. 8(a) and (b)), which was consistent with the OM observations (Fig. 5). It should be noticed that the unDRXed region was almost red, signifying that the ⟨0001⟩ direction was oriented towards compression direction. However, the DRXed regions showed different colors, indicating that grain orientation was randomized after dynamic recrystallization.

The (0001) pole figures are also presented in Fig. 8. Generally, the basal slip is preferentially activated during deformation and promotes grain rotation in a certain direction to form basal texture in Mg alloys [35]. In the present study, compression deformation can rotate the basal planes of the Mg−Zn−Ce alloy perpendicular to the compression direction (CD). Therefore, the as-compressed

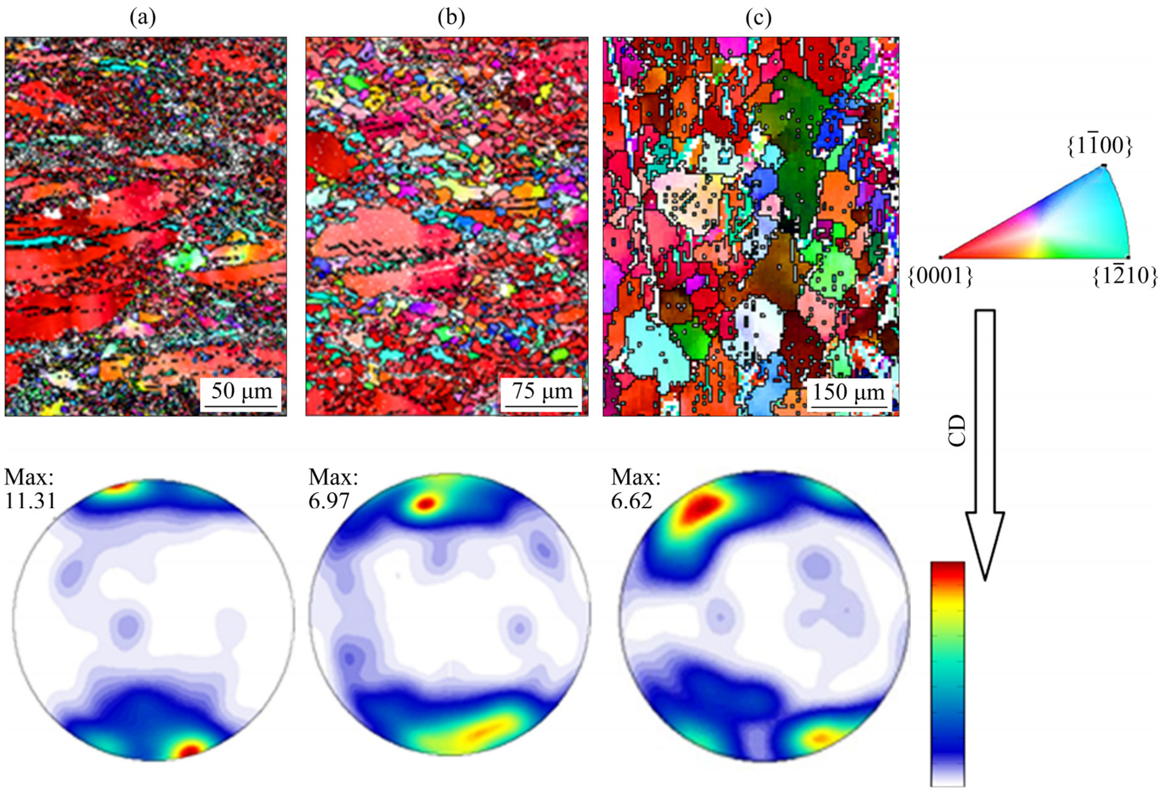

Fig. 8 IPF images and their corresponding (0001) pole figures under different deformation conditions: (a) ln Z=25.5; (b) ln Z=20.77; (c) ln Z=16.43 (CD represents compression direction)

samples exhibited a basal texture. Concurrently, the texture intensity was continuously weakened with decreasing Z parameters. Deformation parameters significantly affected texture evolution of RE-containing Mg alloys [14]. It has been reported that extrusion at low temperature (300 °C) inhibits the formation of the RE texture component in the Mg−Zn−Ce alloy [15] because of the hard activation of non-basal slip deformed at low extrusion temperature. However, RE texture was not detected in the Mg−Gd alloy deformed at high temperatures [14], which was considered to be the prohibition of shear bands at high temperatures. The difference of texture intensity in the Mg−Zn−Ce alloy of the present study should be related to the extent of dynamic recrystallization during hot deformation. The recrystallization region exhibited a weaker texture compared with the unDRXed region of the Mg alloys [36]. That texture intensity was gradually decreased with the decreasing unDRXed zone in the ZK series alloys [37]. XIA et al [38] believed that dynamic recrystallization was a main factor in weakening the texture intensity in Mg−6.8Gd−4.5Y−1.1Nd−0.5Zr (wt.%) alloy. This indicated that texture weakening in Mg alloys might result from dynamic recrystallization. In the present study, the DRX regions increased with decreasing Z parameter, which led to a decrease of the overall texture intensity.

To clarify the effects of deformation parameters on recrystallization texture in Mg−Zn−Ce alloys, the DRXed regions for the samples compressed with high Z parameters were separated and the corresponding (0001) pole figures are presented in Fig. 9. The DRXed grain size gradually increased with decreasing Z parameter. Nevertheless, basal texture intensity in the recrystallization regions showed a similar trend (4.80 (Fig. 9(a)) to 6.62 (Fig. 8(c)) in intensity).

Texture weakening in RE-containing Mg alloys was proposed to be related to twinning inducing nucleation [11], shear band inducing nucleation [39] and solute segregation at grain boundaries or stacking faults [40]. Although the physical mechanism of texture weakening in Mg alloys is still controversial, it is generally accepted that the development of recrystallization texture is determined by the oriented nucleation theory and/or the oriented growth theory [41]. In the oriented nucleation theory, a specific grain orientation

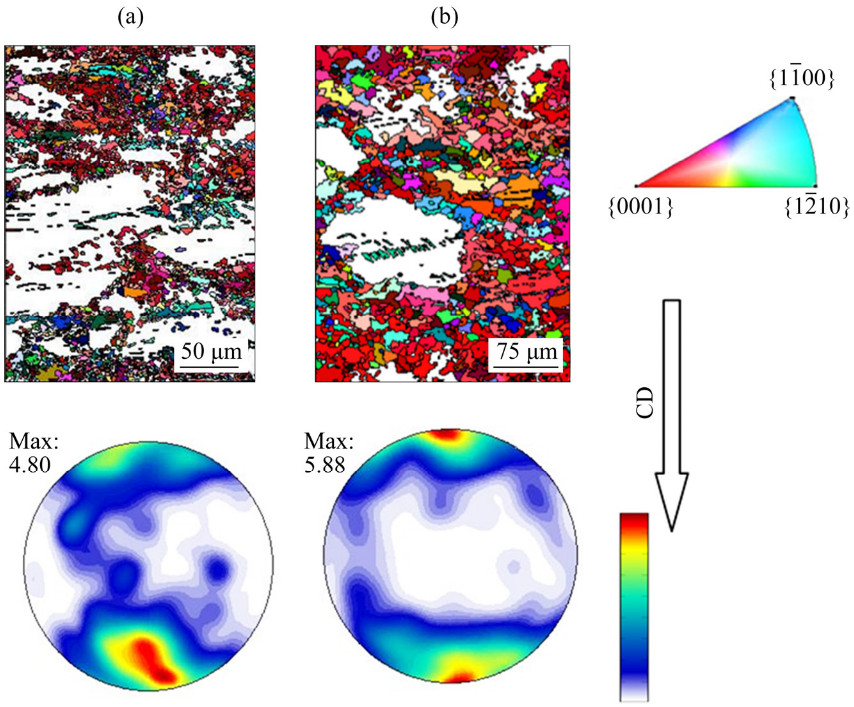

Fig. 9 DRXed regions and their corresponding (0001) pole figures under different deformation conditions: (a) ln Z=25.5; (b) ln Z=20.77 (CD represents compression direction)

formed and remained stable during subsequent grain growth. However, the oriented growth theory proposes that the orientation dependence of the grain boundary mobility is responsible for the recrystallization texture. In the present study, the sample (ln Z=25.5) with the finest DRXed grain size of about 3 μm exhibited a weaker texture intensity (Fig. 9(a)), while the intensity was strengthened with increasing DRXed grain size (Fig. 9(b)). It seems that the preferred grain growth led to an increase in texture intensity. Previous investigations have suggested that DXRed grain size is an important factor in forming RE texture component in RE-containing Mg alloys [42]. WU et al [43] detected that basal-oriented grains have grain growth advantage over other oriented grains in Mg alloys. The reduction in grain boundary energy is the driving force for grain growth. HOLM et al [44] suggested that texture development was associated with grain boundary anisotropy. The basal-oriented grains have low grain boundary energy compared with the non-basal grains, because of the close atomic arrangement in the basal planes. HUANG et al [45] showed that solute atoms were preferentially segregated to high-energy grain boundaries to reduce the grain boundary energy. Therefore, the solute atom Ce with a large atomic radius in the Mg−Zn−Ce alloy contrasts with the Mg atom and segregates to off-basal oriented grains. As a result, the grain boundary mobility of the off-basal oriented grains is reduced. In contrast, basal-oriented grains can grow more easily during grain growth, which contributes to the enhancement of the (0001) texture intensity with increasing of DRXed grains. Moreover, RIOS et al [46] indicated that the activation energy of high-angle grain boundary mobility is much smaller than that of low-angle grain boundary mobility. Therefore, high-angle grain boundaries would have high mobility compared to low-angle boundaries. Consequently, the basal oriented grains prefer to growing towards the off-basal grains during grain growth. Based on the above discussion, it is inferred that texture strengthening is related to the preferred grain growth.

The present study revealed that the microstructure of the compressed Mg−Zn−Ce alloy differed significantly when deformed with different Zener−Hollomon parameters. A bimodal microstructure was obtained when compressed with high Z parameters, in which the unDRXed region exhibited a stronger texture intensity and the DRXed region showed a weaker texture. This inhomogeneous microstructure and strong texture intensity in the unDRXed regions deteriorated ductility. Nevertheless, the texture intensity increased with increasing the DRXed grain size. The microstructure characteristics provide a way to fabricate high performance Mg alloys with high strength and ductility, i.e. obtaining a complete DRXed microstructure with fine grains. Therefore, how to reduce the fraction of unDRXed regions and control the DRXed grain size is essential to achieve superior properties, which will be further investigated.

4 Conclusions

(1) The dynamic recrystallization and texture of the Mg−Zn−Ce alloy were affected significantly by deformation parameters.

(2) Higher Zener−Hollomon parameter resulted in larger fraction of deformed regions and finer dynamically recrystallized (DRXed) grain sizes.

(3) Texture intensity in the unDRXed regions was stronger compared to that in the DRXed regions, which contributed to a sharper texture intensity in the samples deformed with higher Zener−Hollomon parameter.

(4) The recrystallized texture was intensified with increasing grain size, which was attributed to the preferred grain growth.

References

[1] CHENG Yuan-fen, DU Wen-bo, LIU Ke, FU Jun-jian, WANG Zhao-hui, LI Shu-bo, FU Jin-long. Mechanical properties and corrosion behaviors of Mg−4Zn−0.2Mn−0.2Ca alloy after long term in vitro degradation [J]. Transactions of Nonferrous Metals Society of China, 2020, 30: 363−372.

[2] WANG X J, XU D K, WU R Z, CHEN X B, PENG Q M, JIN L, XIN Y C, ZHANG Z Q, LIU Y, CHEN X H, CHEN G, DENG K K, WANG H Y. What is going on in magnesium alloys? [J]. Journal of Materials Science & Technology, 2018, 34: 245−247.

[3] ZHANG Yang, CHEN Xiao-yang, LU Ya-lin, LI Xiao-ping. Microstructure and mechanical properties of as-extruded Mg−Sn−Zn−Ca alloy with different extrusion ratios [J]. Transactions of Nonferrous Metals Society of China, 2018, 28: 2190−2198.

[4] JIA Qing-gong, ZHANG Wei-xi, SUN Yi, XU Chun-xian, ZHANG Jin-shan, KUAN Jun. Microstructure and mechanical properties of as-cast and extruded biomedical Mg−Zn−Y−Zr−Ca alloy at different temperatures [J]. Transactions of Nonferrous Metals Society of China, 2019, 29: 515−525.

[5] LIU Ke, LIU Jin-xue, LI Shu-bo, WANG Zhao-hui, DU Wen-bo, QANG Qing-feng. Effects of secondary phases on texture and mechanical properties of as-extruded Mg−Zn−Er alloys [J]. Transactions of Nonferrous Metals Society of China, 2018, 28: 890−895.

[6] GIFFITHA D. Explaining texture weakening and improved formability in magnesium rare earth alloys [J]. Materials Science and Technology, 2015, 31: 10−24.

[7] ZHAO Hong-liang, HUA Yun-xiao, DONG Xiang-lei, XING Hui, LU Yan-li. Influence of trace Ca addition on texture and stretch formability of AM50 magnesium alloy sheet [J]. Transactions of Nonferrous Metals Society of China, 2020, 30: 647−656.

[8] BALL E A, PRANGNELL P B. Tensile−compressive yield asymmetries in high strength wrought magnesium alloys [J]. Scripta Metallurgica et Materialia, 1994, 31: 111−116.

[9] HIRSCH J, AL-SAMMAN T. Superior light metals by texture engineering: Optimized aluminum and magnesium alloys for automotive applications [J]. Acta Materialia, 2013, 61: 818−843.

[10] STANFORD N. Micro-alloying Mg with Y, Ce, Gd and La for texture modification—A comparative study [J]. Materials Science and Engineering A, 2010, 527: 2669−2677.

[11] HANTZSCHE K, BOHLEN J, WENDT J, KAINER K U, YI S B, LETZIG D. Effect of rare earth additions on microstructure and texture development of magnesium alloy sheets [J]. Scripta Materialia, 2010, 63: 725−730.

[12] ZENGIN H, TUREN Y. Effect of La content and extrusion temperature on microstructure, texture and mechanical properties of Mg−Zn−Zr magnesium alloy [J]. Materials Chemistry and Physics, 2018, 214: 421−430.

[13] ROBSON J D, TWIER A M, LORIMER G W, ROGERS P. Effect of extrusion conditions on microstructure, texture, and yield asymmetry in Mg–6Y–7Gd–0.5wt%Zr alloy [J]. Materials Science and Engineering A, 2011, 528: 7247−7256.

[14] STANFORD N, BARNETT M R. The origin of “rare earth” texture development in extruded Mg-based alloys and its effect on tensile ductility [J]. Materials Science and Engineering A, 2008, 496: 399−408.

[15] CHINO Y, HUANG X S, SUZUKI K, SASSA K, MABUCHI M. Texture and mechanical properties of Mg−Zn−Ce alloy extruded at different temperatures [J]. Materials Transaction, 2011, 52: 1104−1107.

[16] IMANDOUST A, BARRET C, OPPEDAL A, WHITTINGTON W, PAUDEL Y, KADIRI H. Nucleation and preferential growth mechanism of recrystallization texture in high purity binary magnesium−rare earth alloys [J]. Acta Materialia, 2017, 138(Supplement C): 27−41.

[17] WU L B, LIU X H, WU R Z, CUI C L, ZHANG J H, ZHANG M L. Microstructure and tensile properties of Mg–Li–Al–Zn based alloys with Ce addition [J]. Transactions of Nonferrous Metals Society of China, 2012, 22: 779−785.

[18] CHAI Yan-fu, HE Chao, JIANG Bin, FU Jie, JIANG Zhong-tao, YANG Qing-shan, SHENG Hao-ran, HUANG Guang-sheng, ZHANG Ding-fei, PAN Fu-sheng. Influence of minor Ce additions on the microstructure and mechanical properties of Mg−1.0Sn−0.6Ca alloy [J]. Journal of Materials Science and Technology, 2020, 37: 26−37.

[19] BACHMANN F, HIELSCHER R, SCHAEBEN H. Texture analysis with MTEX-free and open source software toolbox [J]. Solid State Phenomena, 2010, 160: 63−68.

[20] HUANG Ming-li, LI Hong-xiao, DING Hua, REN Yu-ping, QIN Gao-wu, HAO SHI-ming. Partial phase relationships of Mg−Zn−Ce system at 350 °C [J]. Transactions of Nonferrous Metals Society of China, 2009, 19: 681−685.

[21] WEI L Y, DUNLOP G L, WESTENGEN H. The intergranular microstructure of cast Mg−Zn and Mg−Zn−rare earth alloys [J]. Metallurgical and Materials Transactions A, 1995, 26: 1947−1955.

[22] SUN Cui-cui, LIU Ke, WANG Zhao-hui, LI Shu-bo, DU Xian, DU Wen-bo. Hot deformation behaviors and processing maps of Mg–Zn–Er alloys based on Gleeble–1500 hot compression simulation [J]. Transactions of Nonferrous Metals Society of China, 2016, 26: 3123−3134.

[23] SUN Yu, WAN Zhi-peng, HU Lian-xi, REN Jun-shuai. Characterization of hot processing parameters of powder metallurgy TiAl-based alloy based on the activation energy map and processing map [J]. Materials & Design, 2015, 86: 922−932.

[24] MIRZADEH H. Constitutive analysis of Mg–Al–Zn magnesium alloys during hot deformation [J]. Mechanics of Materials, 2014, 77(Supplement C): 80−85.

[25] BHATTACHARYA R, WYNNE B P, RAINFORTH W M. Flow softening behavior during dynamic recrystallization in Mg–3Al–1Zn magnesium alloy [J]. Scripta Materialia, 2010, 67: 277−280.

[26] ZHONG T, RAO K P, PRASAD Y V R K, GUPTA M. Processing maps, microstructure evolution and deformation mechanisms of extruded AZ31-DMD during hot uniaxial compression [J]. Materials Science and Engineering A, 2013, 559: 773−781.

[27] FATEMI-VARZANEH S M, ZAREI-HANZAKI A, BELADI H. Dynamic recrystallization in AZ31 magnesium alloy [J]. Materials Science and Engineering A, 2007, 456: 52−57.

[28] SPIGARELLI S, EHTEDI M E, CABIBBO M, EVANGELISTA E, KANEKO J, JAGER A, GARNEROVA V. Analysis of high-temperature deformation and microstructure of an AZ31 magnesium alloy [J]. Materials Science and Engineering A, 2007, 462: 197−201.

[29] XU Yan, JU Lian-xi, DENG Tai-qing, YE Lei. Hot deformation behavior and processing map of as-cast AZ61 magnesium alloy [J]. Materials Science and Engineering A, 2013, 559: 528−533.

[30] ZHOU H T, LI Q B, ZHAO Z K, LIU Z C, WEN S F, WANG Q D. Hot workability characteristics of magnesium alloy AZ80—A study using processing map [J]. Materials Science and Engineering A, 2010, 527: 2022−2026.

[31] LIU Liu-fa, DING Han-lin. Study of the plastic flow behaviors of AZ91 magnesium alloy during thermo-mechanical processes [J]. Journal of Alloys and Compounds, 2009, 484: 949−956.

[32] CICCARELLI D, ELMEHTEDI M, JAGER A, SPIGARELLI S. Analysis of flow stress and deformation mechanism under hot working of ZK60 magnesium alloy by a new strain-dependent constitutive equation [J]. Journal of Physics and Chemistry of Solids, 2015, 87: 183−195.

[33] WATANABE H, TSUTSUI H, MUKAI T, ISHIKAWA K, OKANDA Y, KOHZU M, HIGASHI K. Grain size control of commercial wrought Mg−Al−Zn alloys utilizing dynamic recrystallization [J]. Materials Transaction, 2001, 42: 1200−1205.

[34] XIAO Hong-chao, TANG Bei, LIU Chu-ming, GAO Yong-hao, YU Shi-lun, JIANG Shu-nong. Dynamic precipitation in a Mg–Gd–Y–Zr alloy during hot compression [J]. Materials Science and Engineering A, 2015, 645: 241−247.

[35] AGNEW S R, YOO M H, TOME C N. Application of texture simulation to understanding mechanical behavior of Mg and solid solution alloys containing Li or Y [J]. Acta Materialia, 2001, 49: 4277−4289.

[36] ZHANG Du-xiu, YANG Xu-yue, SUN Huan, LI Yi, WANG Jun, ZHANG Zhi-rou, YE You-xiong, SAKAI Ta-ku. Dynamic recrystallization behaviors and the resultant mechanical properties of a Mg–Y–Nd–Zr alloy during hot compression after aging [J]. Materials Science and Engineering A, 2015, 640: 51−60.

[37] LIU Li-zi, CHEN Xian-hua, PAN Fu-sheng, TANG Ai-tao, WANG Xiao-long, LIU Juan, GAO Shang-yu. Microstructure, texture, mechanical properties and electromagnetic shielding effectiveness of Mg–Zn–Zr–Ce alloys [J]. Materials Science and Engineering A, 2016, 669: 259−268.

[38] XIA Xiang-sheng, ZHANG Kui, LI Xing-gang, MA Ming-long, LI Yong-jun. Microstructure and texture of coarse-grained Mg−Gd−Y−Nd−Zr alloy after hot compression [J]. Materials & Design, 2013, 44: 521−527.

[39] BASU I, AL-SAMMAN T. Triggering rare earth texture modification in magnesium alloys by addition of zinc and zirconium [J]. Acta Materialia, 2014, 67: 116−133.

[40] KIM Y M, MENDIS C, SASASKI T, LETZIG D, PYCZAK F, HONO K, YI S B. Static recrystallization behaviour of cold rolled Mg−Zn−Y alloy and role of solute segregation in microstructure evolution [J]. Scripta Materialia, 2017, 136: 41−45.

[41] DOHERTY R. Nucleation and growth kinetics of different recrystallization texture components [J]. Scripta Metallurgica, 1985, 19: 927−930.

[42] BOHLEN J, YI S B, LETZIG D, KAINER K. Effect of rare earth elements on the microstructure and texture development in magnesium−manganese alloys during extrusion [J]. Materials Science and Engineering A, 2010, 527: 7092−7098.

[43] WU W X, JIN L, ZHANG Z Y, DING W J, DONG J. Grain growth and texture evolution during annealing in an indirect-extruded Mg−1Gd alloy [J]. Journal of Alloys and Compounds, 2014, 585: 111−119.

[44] HOLM E A, HASSOLD G N, MIODOWNIK M A. On misorientation distribution evolution during anisotropic grain growth [J]. Acta Materialia, 2001, 49: 2981−2991.

[45] HUANG X S, SUZUKI K, CHINO Y. Static recrystallization behavior of hot-rolled Mg−Zn−Ce magnesium alloy sheet [J]. Journal of Alloys and Compounds, 2017, 724: 981−990.

[46] RIOS P R, JR F S, SANDIM H R Z, PLAUT R L, PADILHA A F. Nucleation and growth during recrystallization [J]. Materials Research, 2005, 8: 225−238.

变形参数对 Mg−Zn−Ce 合金显微组织和织构的影响

杜玉洲 [1,2]，刘东杰 [1,2]，葛延峰 [1,2]，蒋百灵 [1,2]

1. 西安理工大学 科学与工程学院，西安 710048；
2. 西安理工大学 陕西省镁合金工程技术中心，西安 710048

摘　要：采用 Gleeble−1500 热模拟试验机在不同温度(250, 300, 350 °C)和应变速率(0.001, 0.01, 0.1 s^{-1})下对 Mg−6Zn−0.5Ce (质量分数，%)合金进行热压缩试验，采用光学显微镜和电子背散射衍射技术研究热压缩变形过程中合金的显微组织和织构演变。结果表明，由变形工艺决定的 Zener−Hollomon 参数对 Mg−6Zn−0.5Ce 合金的动态再结晶和织构具有重要影响。随着 Zener−Hollomon 参数的增大，未再结晶区的体积分数增大且动态再结晶晶粒尺寸减小。再结晶区的织构强度弱于未再结晶区的织构强度，这使经较高 Zener−Hollomon 参数变形的试样呈较高的织构强度。再结晶织构强度的增加与晶粒择优生长有关。

关键词：Mg−Zn−Ce 合金; 热变形; 织构演变；动态再结晶

(Edited by Wei-ping CHEN)